Materials Physics and Mechanics. 2022;49(1): 145-152
Conference materials
http://dx.doi.org/10.18149/MPM.4912022_10

Emergence of topological defects in a bilayer of multiwalled carbon nanotubes irradiated by gamma-rays

H.V. Grushevskaya✉, A.I. Timoshchenko, I.V. Lipnevich

Physics Faculty, Belarusian State University, 4 Nezaleznasti Ave., Minsk, Republic of Belarus

✉ grushevskaja@bsu.by

Abstract. We have studied gamma-ray scattering on rolled graphene atomic layers of high-ordered multiwalled-carbon-nanotubes which organized a bilayer. Radiation high-energy topological defects of a type of pair "vortex-antivortex" in electron and hole densities have been revealed. We suppose that the fluxes of the vortex-antivortex pairs are produced by gamma-quanta in the graphene plane.
Keywords: carbon nanotube, gamma-ray scattering, radiation defect

Acknowledgements*. No external funding was received for this study.*

Citation: Grushevskaya HV, Timoshchenko AI, Lipnevich IV. Emergence of topological defects in a bilayer of multiwalled carbon nanotubes irradiated by gamma-rays. *Materials Physics and Mechanics*. 2022;49(1): 145-152. DOI: 10.18149/MPM.4912022_10.

1. Introduction

Among applications of graphene-like materials in nuclear technologies, the development of radiation-resistant materials and of protective shielding nanostructured coatings are in great demand. Graphene is stable to irradiation because the knocked-on neutral carbon atoms reside on the graphene plane. The radiation resistance of graphene can be caused by an interaction of gamma-quanta with the graphene charge vortical carriers of the pseudo-Majorana type [1,2]. A mechanism of the interaction between gamma-quanta and the pseudo-Majorana charge carriers in the graphene plane leading to a Compton scattering on super-dense fluxes of the pseudo-Dirac charge carriers has been not ascertained yet.

In the paper, we will study gamma-ray scattering on rolled graphene atomic layers of high-ordered multiwalled-carbon-nanotubes (MWCNTs) which organized a bilayer. Our goal is to reveal radiation high-energy topological defects of a type of pseudo-Majorana pairs "vortex-antivortex" in graphene electron and hole densities.

2. Materials

MWCNT bundles were fabricated utilizing Langmuir-Blodgett (LB) nanotechnique. The carboxylated and stearic-acid-functionated MWCNTs under 2.5–5 nm in diameter have been decorated by nanocyclic complexes (Fe(II)DTP) of Ce and/or high-spin octahedral Fe with ligands being conducting oligomer of dithionylpyrrole series in the following way. As a preliminary, an alkyl hydrocarbon chain $C_{16}H_{33}$ was linked chemically to the oligomer. Chemical formula of the oligomer has the following form: 3-hexadecyl-2.5-di(thiophen-2-yl)-1H-pyrrole (H-DTP). A 5-monolayer graphene-like film of the nanocyclic organometallic complexes is fabricated by means of LB-nanotechnique. Then, inverse micelles of stearic acid

Publisher: Peter the Great St. Petersburg Polytechnic University

with MWCNTs inside are obtained by mixing stearic acid and MWCNTs in hexane by the ultrasound treatment, and the 2-monolayer MWCNT films fabricated from these micellar MWCNTs by the LB-nanotechnique are deposited on the nanocyclic-complex LB-cover.

We have used the planar capacitive sensor of interdigital-type on such glass-ceramic support as pyroceramics [3]. N_e pairs, N_e = 20, of aluminium electrodes of the sensors are arranged in an Archimedes-type spiral configuration. Every such pair is an "open type" capacitor. The dielectric coating of the electrodes represents itself nanoporous anodic alumina (AOA) with a pore diameter of 10 nm. The MWCNT LB-bundles decorated by organometallic complexes or the LB-films of nanocyclic organometallic complexes were deposited on the interdigital structure of aluminium electrodes, on the surface of which the AOA layer was previously formed.

3. Methods

Exposure to radiation and radiation spectroscopy. The standard low-intensive source of ionizing radiation (IRS) ^{137}Cs (CsJ) was utilized. A low-intensive beta-particles beam from IRS has been attenuated by a thin-film aluminium shield. The radiation source has the form of a drop with an average diameter of about d = 1.5 mm. An absolute IRS activity A_0 equal to 124.4 kBq on the date 1 April 1990 was quoted to about 1% precision. A sample with a diameter D = 4 mm is exposed through the lead collimator being of the order of 5 mm in diameter and L = 25, 50 mm long. The IRS is placed above the collimator. At the ratio $d / L = 0.03, 0.06$ the IRS can be considered a point source. Then an estimate of the fluence rate φ_0 for the primary gamma radiation within the irradiated sample gives $\varphi_0 = 8.5\ 10^3\ m^{-2}s^{-1}$ at $d / L = 0.03$ in supposing that the percentage of the emitted photons per one decay (quantum yield) is equal to 0.851 for the IRS ^{137}Cs. The fluence-increase factor is 24 for $d / L = 0.06$. A number of gamma quanta coincide with a number of 0.512 MeV electrons emitted by ^{137}Cs atoms in the decay process. Since the percentage of 1.174 MeV electrons is of 5.3 %, the fluence of beta-quanta with the energy 1.174 MeV is less than 485 $m^{-2}s^{-1}$ at $d / L = 0.03$. MWCNTs were exposed to radiation for 1 or 3 hours at $d / L = 0.03$ and 86 min at $d / L = 0.06$. Accordingly, we have registered approx 9200 events at $d / L = 0.06$. A graphene monolayer deposited on an insulator surface becomes conducting under action of β-radiation [4]. But, since in our case the intensity of the beta rays is very small due to aluminium shield, the doping of the MWCNT layer is negligible.

An analysis of secondary electrons spectra has been performed by a lab-quality radiation spectrometric facility "Nuclear Physics" (BSU, Minsk, Belarus). The scintillation crystal thallium-activated sodium iodide, NaI(Tl) (diameter of 25 mm, height of 40 mm)) was utilized as a detector crystal. A photoelectric-multiplier supply voltage U changes from 100 to 1000 V; the number of channels (a maximal pulse height) is 1024; the integral nonlinearity (transducer characteristic error) is less than 0.1%.

Impedance measurements. Electrophysical properties of the ultra-thin LB-films were studied by means of the impedance spectroscopy methods as a variation in dielectric polarization of a Helmholtz double electrically-charged layer formed at the interface between a surface of the fabricated electrochemical sensor and water. Electrochemical measurements were carried out in deionized water at room temperature.

The non-faradic impedimetric sensor operates on surface-polarization-decreasing effects originated by the conducting ultra-thin LB-layers screening the electrodes. The dielectric losses ε'' due to a dielectric-polarization relaxation process occur in a frequency range where the sensor capacitance C falls down. The ε'' is the imaginary part of the complex dielectric permittivity $\varepsilon = \varepsilon' + i\varepsilon''$, and, correspondingly, presents a resistivity because
$\varepsilon'' = \Re e\, \sigma / \omega = \Re e\, (\sigma V) / (\omega V) \sim I / V.$

Here I and V are the electrical current and bias, respectively; σ is the conductivity. Then, as Figure 1 (at the left) shows, the discharging (charging) current I_{ch} emerges producing the bias

$V \sim \varepsilon'' I_{ch}$

in an RC oscillator. The V determines the energy $CV^2/2$ stored at (released from) the capacitance change C/T as

$CV^2/2 \sim I_{ch} VT$,

where T is the charging-process duration. Substituting the expression for the V into the expression for the energy, one can assume that

$\varepsilon'' \sim T/C$.

The signal power W/T recorded by the Fourier analyzer is proportional to the dielectric dispersion ε' because W is the stored energy determined by the following equation:

$W \sim T\vec{D} \times \vec{H}$

with the electric displacement vector $\vec{D} = \varepsilon' \vec{E}$, where $\vec{E}$ and $\vec{H}$ are the electric and magnetic fields vectors, respectively.

Let us suppose that N dipole-polarization processes proceed inside of the Helmholtz layer emerging near the electrodes. It signifies that an equivalent circuit diagram of both the capacitor-charging (capacitor-discharging) and polarization processes consists of N+1 RC circuits. The equivalent circuit of the sensor is presented in Fig. 1 (at the right).

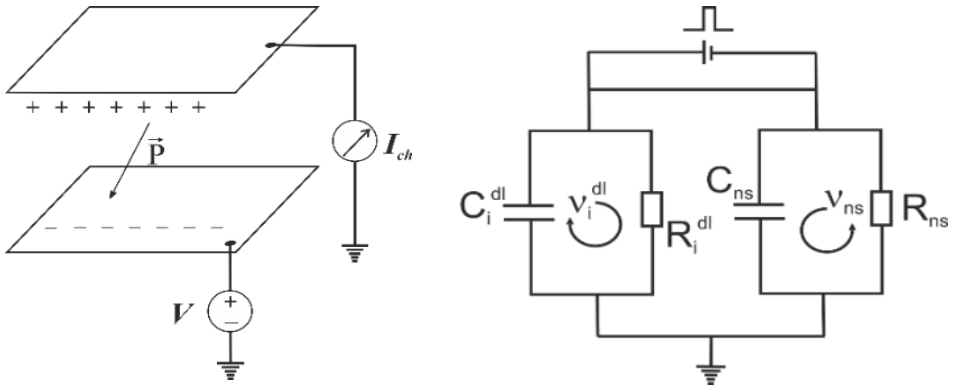

Fig. 1. Scheme of the sensor operation based on a dielectric-polarization relaxation process and an equivalent circuit diagram of the sensor. A square voltage pulse with a bias is applied to the sensor to excite the autooscillations; $\vec{P}$ is the polarization vector

As one can see in Fig. 1 (at the right), forced oscillations with a frequency ν_i can be generated in the i-th parallel circuit for which the double-layer resistance $R_i^{dl} \equiv R_i$ i=1,…, N is much less than the instrument resistance $R_{ns} = R_{N+1}$ in some frequency range $\nu_i \pm \Delta_i$. If $R_i < R_{ns}$ $i \neq 1,\ldots, N$, then the forced oscillations with a frequency $\nu_{ns} \equiv \nu_{N+1}$ are generated in the properly measuring (N+1)-th RC circuit. Thus, the dependence of T/C on WT will present N Cole-Cole plots and one Nyquist impedance plot for parallel connection of the capacitor to the instrument resistor R_{ns} (see Fig. 2).

To excite harmonic auto-oscillations of electric current (charge-discharge (charging) processes in the capacitors), the sensor was connected as the capacitance C into the relaxation resistance-capacitance oscillator (self-excited RC-oscillator) [5]. A self-excitation of an amplifier with positive feedback occurs in such RC-oscillator on quasiresonance frequencies. The capacitance change C/T of the sensor, entered measuring RC-oscillating circuit, has been calculated by the formula $C/T = 1/(2\pi R_{ns} f)$, where f is a quasi-resonance frequency.

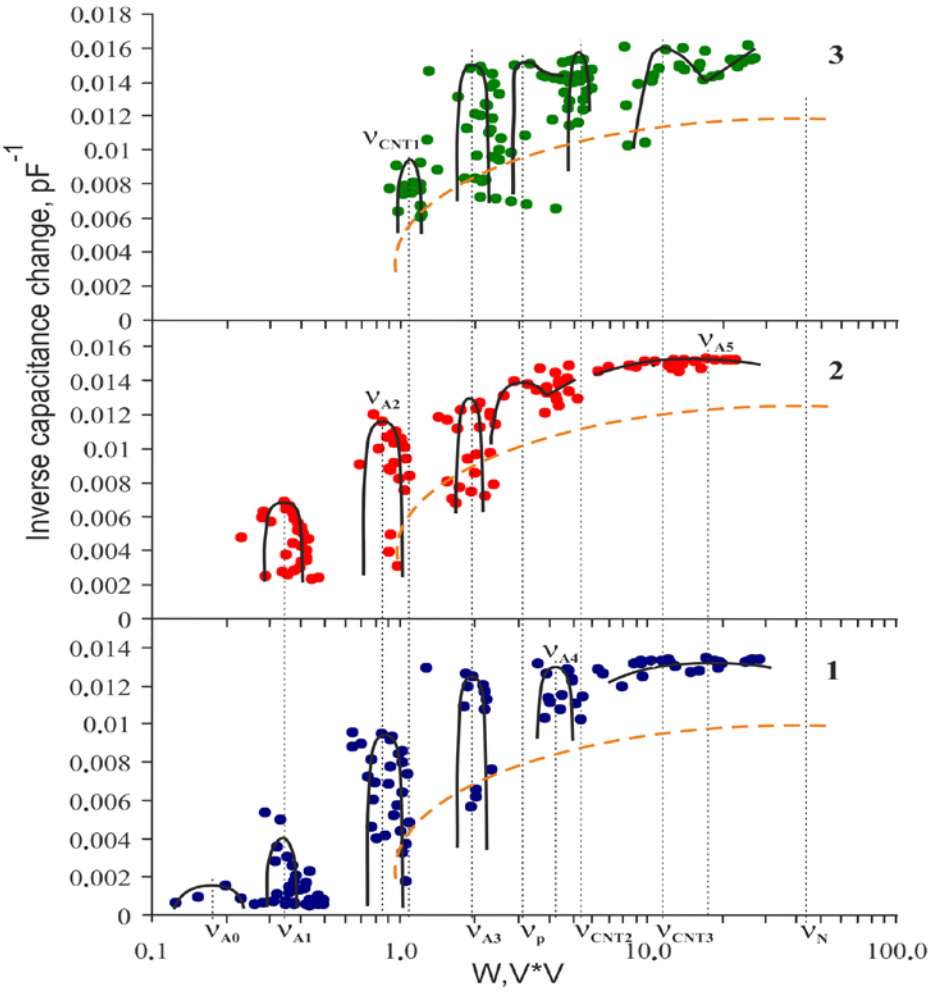

Fig. 2. Dielectric spectra: 1) for nanoporous AOA, 2) and 3) for nanoheterostructure based on Ce-containing nanocyclic compound Fe(II)DTP and on decorated MWCNTs, respectively. Quasiresonance frequencies ν of Cole-Cole plots in the spectra are marked as ν_{Ai}; i = 0, …, 5 for AOA; ν_P for the organometallic compound and ν_{CNTi}; i = 1,2,3 for MWCNTs. Nyquist plot of impedance for the measuring circuit is marked by a yellow dash line with ν_N

4. Analysis of radiation spectra

Response functions of the detector with and without the absorber are shown in Fig. 3. The radiation spectrum of CsJ is a typical one recorded from the NaI(Tl) scintillation detectors. The IRS response function R_{Cs} feature peaks of photoelectric absorption (photopeak) and a characteristic X-ray at the lower and highest pulse heights respectively. The characteristic X-ray photons are emitted by free electrons filling non-occupied electron *K*-shells in atoms of the lead collimator. The photopeak appears at the energy of the original ^{137}Cs gamma-ray photon. A Compton scattering gives rise to a single Compton continuum of energies and multiple-Compton-scattering events in the IRS spectra. The multiple Compton scattering occurs due to the sufficiently large size of the detector crystal. One observes also a peak caused by the bremsstrahlung generated in stopping the beta particles by the IRS shield and the backscatter peak caused by photons Compton scattered at large angles in materials immediately surrounding the scintillator crystal (see Fig. 3a).

Radiation background has been subtracted from original distributions; the exposure lasted 86 min at $d / L = 0.06$. The backscatter peak, the photopeak, the characteristic X-ray

peak, and the contribution from the bremsstrahlung are labeled by "BS", "Ph", "X", and "Brem", respectively; the absorber escape peaks of the pseudo-Majorana chiral, semichiral, nonchiral fermions, which are created at the interaction between graphene and gamma-ray, are designated as "V_{ch}", "V_{sc}", and "V_{nc}", respectively. The single Compton continuum and the area of multiple Compton scattering are labeled by "Single Compton" and "Multiple Compton", respectively.

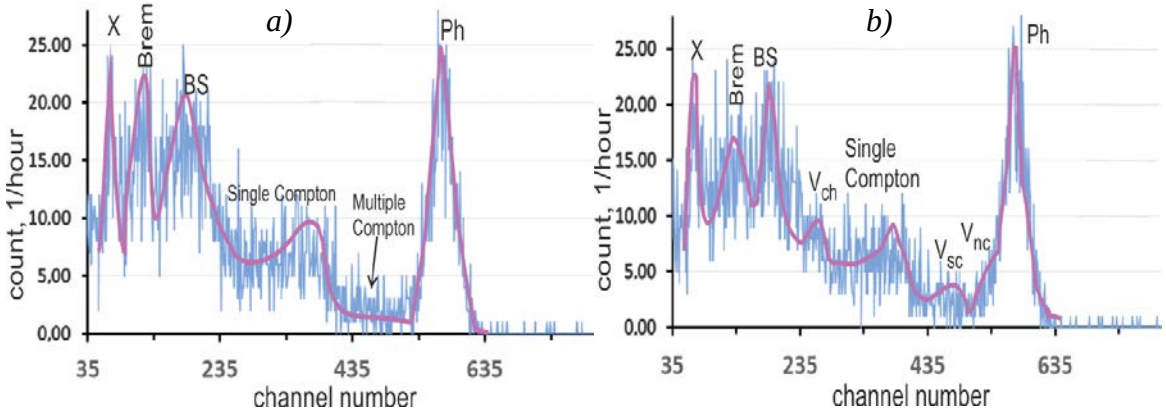

Fig. 3. Pulse height spectra R_{Cs} (*a*) and R_{CsG} (*b*) for photon beam incoming from IRS ^{137}Cs through the collimator without and with an absorber, respectively, and scattering on a detector crystal

Let us analyze MWCNT effects on the incoming ^{137}Cs gamma-quanta beam. After placing the electromagnetic-radiation absorber with the bilayer of ordered MWCNT bundles decorated by the organometallic compound into the collimator, three additional peaks reveal themselves in the ^{137}Cs-radiation spectrum of secondary electrons along with the photopeak, the single Compton continuum, the backscatter peak, the X-ray escape peak, and the bremsstrahlung. The spectra indicate narrowing of the ^{137}Cs-radiation peaks. The shape of the single Compton continuum of ^{137}Cs-radiation spectrum has a maximum being approximately in the 360th channel after placing the MWCNT sample into the collimator. Maxima of the three new peaks are approximately in the 260th, 460th, and 535th channels. It testifies that in creating pairs of charge carriers in graphene, the gamma-quanta escape from the detector. Collisions between the radiation defects of graphene and the photons of bremsstrahlung lead to decreasing the peak "Brem".

Now we will utilize the experimental data to elucidate a pseudo-Majorana nature of the graphene charge carriers. To do it, we offer the following mechanism of graphene radiation resistivity. The resistivity is generated by the creation of neutral vacancies V^0 with knocked-on neutral carbon atoms C^0 fixed on a graphene monolayer by radiation defects of a pseudo-Majorana type. The gamma-rays can escape from the detector crystal owing to the production of radiation-defect pairs. The pairs consist of topologically nontrivial defects of delocalized electron (hole) density in one part of the graphene plane and topologically nontrivial defects of hole (delocalized electron) density in another part.

The pseudo-Majorana vortex-antivortex pairs are created at the Compton scattering of the gamma-rays on the MWCNT graphene planes. The radiation defects decrease the energy deposited in the detector which results in the appearance of the additional peaks V_{ch}, V_{sc}, and V_{nc} in the response function R_{CsG} (see Fig. 3b). At colliding with carbon atoms the free pseudo-Majorana fermions are de-excited and confined by hexagonal symmetry near the Dirac touching valent and conductivity graphene bands. Meanwhile, the graphene pseudo-Majorana band structure has degenerated and the vortex pairs transit from the flat area to the

conical one of the graphene band. It signifies that the branches of the vortex begin to move inconsistently. The vortex decay leads to the emergence of an electron-hole avalanche.

5. Impedance analysis

Dielectric spectra of non-exposed structures under investigation are presented in Fig. 2. Unlike graphene-like materials, the dielectric spectra of anodic alumina (AOA) do not have specific dielectric Cole-Cole plots with a diffuse element or Warburg impedance Z_W. Since the Warburg impedance is absent for AOA and, consequently, aluminium-electrodes oxidation does not happen, the fabricated nanoheterostructures are stable. The Cole-Cole plot for metal-containing dithionylpyrrole LB-films testifies both the Warburg impedance element Z_W of a diffuse layer, in which the electrochemical reactions with mass transfer proceed and an electric capacity of the Helmholtz double layer. For the dithionylpyrrole LB-films, this oxidation-reduction potential is stipulated by a change of molecular-group charge state which arises due to self-redox activity of pyrrole residue and electrical charge transport along the chain of conjugated double bonds According to the Cole-Cole plot of the spectrum with Z_W in Fig. 2, MWCNTs, as LB-DTP-films, are redox self-active. Changing the charge state of valleys $K(K')$ (Dirac points) of the graphene Brillouin zone in the momentum space is associated with the mass transfer that Kitaev-like chains with Majorana end states emerge. Meanwhile, the plasma oscillations of produced electron-hole pairs shield the electric field of charged electrodes.

The frequency dependences of electrical capacity for the two materials studied are shown in Fig. 4.

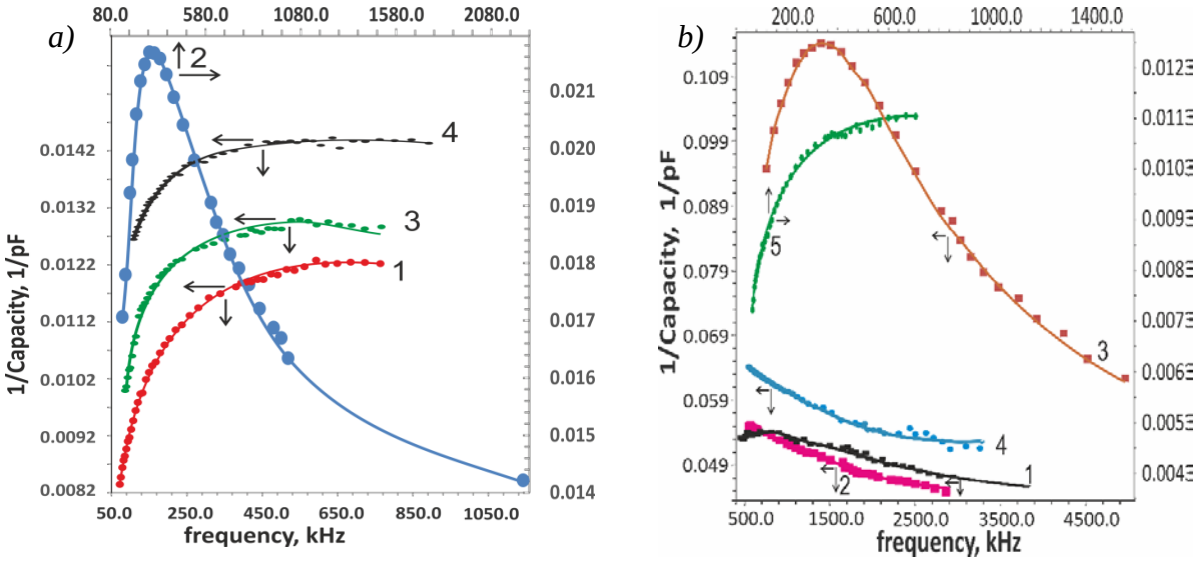

Fig. 4. Frequency dependences of electrical capacity.
(*a*) Fe-containing dithionylpyrrole LB-film:
1) immediately after irradiation, 2) in two weeks after irradiation, 3) in three months after irradiation, 4) before irradiation; the duration of irradiation was 1 hour at $d / L = 0.03$.
(*b*) MWCNTs decorated by nanocyclic complexes of Fe and Ce with dithionylpyrrole ligands.
1) immediately after irradiation, 2) in 24 hours after irradiation, 3) in three weeks after irradiation, 4) in four months after irradiation, 5) before irradiation; the duration of irradiation was 3 hours at $d / L = 0.03$

According to Bode capacity plots 1, 2, and 4 in Figure 4a for irradiated and non-irradiated organometallic-compound LB-films, the dipole relaxation of radiation-vacancy clusters is observed simultaneously with increasing the shielding degree two weeks after the

irradiation by the weak gamma-ray fluence from IRS ^{137}Ce at $d / L = 0.03$. The sharp increase of shielding degree indicates that the number of free charge carriers enlarges extremely. Since the electron-hole pairs are charge carriers in graphene and graphene-like materials, the increase in the free charge carrier's density indicates the localization of holes or electrons from electron-hole pairs after irradiation. The incoming particles can collide with electrons only. Since the carbon atoms are knocked out, the holes (vacancies), localized in the Dirac points, remain. The charge density of vacancy ensemble has the form of atom-like density of localized holes surrounded by delocalized electron density. The dipole relaxation of these individual radiation-vacancy ensembles disappears for a long enough time about three months according to the comparison of dielectric spectra 2 and 3 in Fig. 4a. Emerging only two weeks later after the irradiation, the individual atom-like vacancy arrays indicate a decay of very large cluster of radiation vacancies into the small atom-like arrays (artificial atoms) in graphene-like monolayer plane during self-repairing processes.

We submit the following mechanism of emerging clusters of radiation vacancies. Since the gamma rays created by IRS possess high energy, the atom-like ensembles of radiation vacancies are produced in the excited state with non-occupied both valence and internal orbitals. Due to overlapping the external orbitals of such artificial atoms in an excited state, there arise large clusters of radiation vacancies. Hydrate complexes of atom-like structures formed by vacancies are appeared due to the transition of the latter into the ground state after two weeks, as it follows when the Bode plots 1 and 2, Fig. 4a, are compared. This is evidence that the external orbitals in the ground state are not overlapped. The decay of large radiation clusters into the separate artificial atoms (electrically confined quantum dots) is testified by the corresponding resonance at a frequency of 280 kHz for the metal-containing LB-film. The lifetime of an individual quantum dot is very large so the dots exist for one or two months.

Mobile interstitial carbon atoms, being near a monolayer plane, can form chemical cross-links with hydrocarbon alkyl chains. From the frequency dependencies 3 and 4, Fig. 4a, it follows that after the decay of the artificial atoms the sensor electric capacity of metal-containing dithionylpyrrole LB-films only slightly increases. The weak increase is stipulated by destroying the double-bound chains by the cross-links with near-lying alkyl hydrocarbon chains leads to an attenuation of the shielding effect.

The mechanism of MWCNT radiation resistivity is similar to that of metal-containing dithionylpyrrole LB-film. The dielectric spectra of irradiated and non-irradiated LB-films of MWCNTs decorated by nanocyclic complexes of Ce and octahedral high-spin Fe are presented in Fig. 4b. According to Bode plot 3, the dipole relaxation of hydrated atom-like clusters of radiation vacancies occurs at higher frequencies (about 1320 kHz) than in the dithionylpyrrole films. This is due to the restriction of the artificial atom size by the CNT diameter value. According to the Bode plots 1-4, Fig. 4b, the decay of excited radiation-induced artificial-atom aggregates occurs three weeks after irradiation, while the restoration of electrophysical properties of MWCNTs occurs in three months after the irradiation when quasi-stationary artificial atoms disappear. The shift of the maximum in frequency dependence 1, Fig. 4b, towards low frequencies is registered immediately after irradiation too. This shift indicates the formation of atom-like clusters of vacancies under the action of gamma-rays in the metal-containing dithionylpyrrole LB-monolayers decorating MWCNTs. Decreasing the electric capacity of non-irradiated MWCNTs from 85.2 to 18.5 pF is registered immediately after three-hour irradiation. Accordingly, the intensity increase in the Bode plot 1 in respect of plot 5 in Fig. 4b testifies to the high shielding efficiency of MWCNTs-network and, accordingly, its high electric conductivity. It signifies that in the addition to the radiation-resistivity mechanism for metal-containing dithionylpyrrole LB-film there are cross-connections between graphene monolayers of MWCNT and interstitial knocked-out carbon atoms through chemical bonds into a high-shielding network.

The shielding effect of the LB-films is revealed also as the intensity change of Compton scattering (see Fig. 3). Compare the single Dirac continuum in the detector spectrum in the presence of the absorber and without it. We observe a growth of the number of photons at the scattering angle $\theta = \pi$. In accord with the Klein-Nishina formula [6], the number of photons scattered at $\theta = \pi$ grow with decreasing their energy [7]. Thus, as the quasi-relativistic graphene model predicts, the experimental study fulfilled discovered the existence of the Compton effect at irradiation of the graphene-like material.

6. Conclusions

Scattering the 661.7-keV gamma-rays in MWCNTs create pairs of topologically nontrivial radiation defects and antidefects. We assume that these high-energy graphene pairs of scattering centers are pseudo-Majorana vortical and antivortical fermions. Annihilating and scattering on carbon electron density, the pseudo-Majorana quasi-particles avalanche-likely produce electron-hole configurations of graphene charge density.

References

1. Grushevskaya H, Timoshchenko A, Avdanina E, Lipnevich I. Clustering artificial atoms induced by high-frequency electromagnetic radiation in graphene monolayers of multiwalled carbon nanotubes. *Int. J. Nonlinear Phenomena in Complex Systems.* 2020;23(3): 342-356.
2. Grushevskaya H, Krylov G. Vortex dynamics of charge carriers in the quasi-relativistic graphene model: high-energy kp approximation. *Symmetry*. 2020;12(2): 261.
3. Konstantinova TE, Lyafer EI. Hydrostatic compaction pressure influence on sintered spodumene pyroceramics properties. In: Trzeciakowski WT (ed.) *High Pressure Science and Technology*. Singapore: World Scientific Publishing; 1996. p.118-120.
4. Starodubtsev VA, Fursa TV, Zausaeva NN. Charge electrification of irradiated dielectrics and its effect on incident flux. *J. Electrostatics.* 1988;20(3): 341.
5. Abramov II, Hrushevski VV, Krylov GG, Krylova HV, Lipnevich IV, Orekhovskaja TI. A method of impedance calculation for impedimetric sensor with interdigital structure. *Petersburg Electronics J*. 2012;4(73): 59-67.
6. Krajewska K, Vélez FC, Kamiński JZ. Generalized Klein-Nishina formula. *Phys. Rev. A.* 2015;91(6): 062106.
7. Shafroth SM. (ed.) *Scintillation Spectroscopy of Gamma Radiation*. London: Gordon & Breach, Inc.; 1964.

THE AUTHORS

H.V. Grushevskaya
e-mail: grushvskaja@bsu.by
ORCID: 0000-0002-9527-9328

A.I. Timoshchenko
e-mail: TimoshchenkoAI@bsu.by
ORCID: -

I.V. Lipnevich
e-mail: lipnevich@bsu.by
ORCID: -